

## Structural basis of cohesin cleavage by separase

Zhonghui Lin<sup>1,2</sup>, Xuelian Luo<sup>2</sup>, and Hongtao Yu<sup>1,2,\*</sup>

<sup>1</sup>Howard Hughes Medical Institute, University of Texas Southwestern Medical Center, 6001 Forest Park Road, Dallas, TX 75390

<sup>2</sup>Department of Pharmacology, University of Texas Southwestern Medical Center, 6001 Forest Park Road, Dallas, TX 75390

### Abstract

Accurate chromosome segregation requires timely dissolution of chromosome cohesion after chromosomes are properly attached to the mitotic spindle. Separase is absolutely essential for cohesion dissolution in organisms from yeast to man<sup>1,2</sup>. It cleaves the kleisin subunit of cohesin and opens the cohesin ring to allow chromosome segregation. Cohesin cleavage is spatiotemporally controlled by separase-associated regulatory proteins, including the inhibitory chaperone securin<sup>3–6</sup>, and by phosphorylation of both the enzyme and substrates<sup>7–12</sup>. Dysregulation of this process causes chromosome missegregation and aneuploidy, contributing to cancer and birth defects. Despite its essential functions, atomic structures of separase have not been determined. Here, we report crystal structures of the separase protease domain from *Chaetomium thermophilum*, alone or covalently bound to unphosphorylated and phosphorylated inhibitory peptides derived from a cohesin cleavage site. These structures reveal how separase recognizes cohesin and how cohesin phosphorylation by polo-like kinase 1 (Plk1) enhances cleavage. Consistent with a previous cellular study<sup>13</sup>, mutating two securin residues in a conserved motif that partially matches the separase cleavage consensus converts securin from a separase inhibitor to a substrate. Our study establishes atomic mechanisms of substrate cleavage by separase and suggests competitive inhibition by securin.

---

Separase belongs to the clan CD family of cysteine proteases that includes caspases<sup>1</sup>. It contains a large N-terminal armadillo (ARM) repeat domain and a highly conserved C-terminal separase protease domain (SPD) that consists of a pseudo protease domain (PPD) and an active protease domain (APD)<sup>14</sup> (Fig. 1a and Extended Data Fig. 1). Cohesin forms an asymmetric ring to topologically entrap chromosomes (Fig. 1a)<sup>15,16</sup>. Separase cleaves the kleisin subunit to open the cohesin ring and trigger chromosome segregation. It also cleaves

---

Users may view, print, copy, and download text and data-mine the content in such documents, for the purposes of academic research, subject always to the full Conditions of use: [http://www.nature.com/authors/editorial\\_policies/license.html#terms](http://www.nature.com/authors/editorial_policies/license.html#terms) Reprints and permissions information is available at [www.nature.com/reprints](http://www.nature.com/reprints).

\*Correspondence and requests for materials should be addressed to H.Y. (Email: [hongtao.yu@utsouthwestern.edu](mailto:hongtao.yu@utsouthwestern.edu))

**Author Contributions** Z.L. performed all experiments in this study with advice from H.Y. X.L. provided assistance with structure refinement. Z.L. and H.Y. wrote the paper.

Atomic coordinates and structure factors have been deposited in the Protein Data Bank under accession codes 5FBY, 5FC3, and 5FC2.

The authors declare no competing financial interests.

Readers are welcome to comment on the online version of the paper.

other substrates to regulate anaphase spindle elongation and centriole duplication<sup>17,18</sup>. High-resolution structures of separase have not been determined more than a decade since its discovery, hindering our understanding of its mechanism and regulation.

We found that SPD of *Chaetomium thermophilum* (*ct*) separase could be expressed in large quantities in bacteria without securin (Extended Data Fig. 2a). Recombinant *ct*SPD, but not the C2110S mutant, cleaved *ct*Scc1 to produce two major fragments (Extended Data Fig. 2b). Separase is known to cleave after the EXXR (X, any residue) consensus motif<sup>2</sup>. Charge-reversal mutation of the <sup>212</sup>EVGR<sup>215</sup> motif in *ct*Scc1 reduced cleavage by separase (Fig. 1b,c). An acyloxymethyl ketone (AMK)-containing peptide inhibitor derived from this cleavage site blocked *ct*Scc1 cleavage in a dose-dependent manner (Extended Data Fig. 2c,d), and retarded the gel mobility of *ct*SPD<sup>WT</sup>, but not *ct*SPD<sup>C2110S</sup>, consistent with covalent inhibition (Extended Data Fig. 2e). Similar to separases from other species<sup>6</sup>, longer constructs of *ct*SPD containing an N-terminal extension underwent cleavage at the <sup>1643</sup>ELAR<sup>1646</sup> site (Fig. 1b and Extended Data Fig. 2f). Thus, recombinant *ct*SPD was active.

We determined the crystal structure of *ct*SPD (Fig. 1d and Extended Data Table 1). It forms one globular domain with two sub-domains—the pseudo protease domain (PPD) and the active protease domain (APD)—that pack against each other. APD has an overall fold similar to that of caspases (Fig. 1d,e, and Extended Data Fig. 3, 4a). PPD also has a mixed  $\alpha/\beta$  fold, but its central  $\beta$ -sheet has a topology different from that of caspases. One edge of this central sheet of PPD forms an edge-on interaction with that of APD, whereas the other edge is capped by a helical domain in PPD. A prominent helical insert (HI) of PPD forms a long coiled-coil and packs against APD.

The catalytic dyad H2083 and C2110 are located in loops L3 and L4 of APD (Fig. 1d and Extended Data Fig. 3a). An important mechanism of pro-caspase activation is the reorganization of L4, which can be achieved through homo-dimerization, cleavage of an internal linker, or both<sup>19–22</sup>. The geometry of the catalytic dyad and the extended conformation of L4 in *ct*SPD are similar to those in active caspase 9 (Fig. 1d,e), consistent with *ct*SPD being an active enzyme. Thus, separase activation does not require proteolytic cleavage of L4. Consistent with the importance of the L4 loop, mutations of two residues adjacent to C2110, M2108 and S2112, reduced the activity of *ct*SPD (Fig. 2a,b and Extended Data Fig. 4b). In contrast, mutations of L4 residues distal to C2110, including E2120 and F2121, enhanced the activity of *ct*SPD.

A segment of the N-terminal tag of recombinant *ct*SPD binds to a conserved surface pocket in PPD adjacent to L4 (Figs. 1d, 2c, and Extended Data Fig. 4c). Although this tag is not required for the activity of *ct*SPD, mutations targeting residues in the tag-binding pocket altered the activity of *ct*SPD containing the tag (Fig. 2d and Extended Data Fig. 4d). Similar to mutations of the distal L4 residues, the D1698K and D1960K mutations enhanced the activity of *ct*SPD. We propose that securin or other regions of separase may bind to this tag-binding site, alter the conformation of L4, and affect the protease activity of separase. Even without *bona fide* ligands, binding of an artificial tag to this site can regulate the protease activity of *ct*SPD in a subtle way.

Unlike active caspase 9, which forms a homodimer<sup>19</sup>, separase contains an internal PPD in the same polypeptide chain that packs against and stabilizes its APD. In particular, the helical insert (HI) of PPD makes extensive contacts with APD and bridges the two subdomains (Extended Data Fig. 5a,b). Deletion of HI or mutations of key residues at the HI-APD interface, including D1805 and W2143, abolished the expression of soluble *cSPD* in bacteria (Fig. 2e and Extended Data Fig. 5a,c). Several HI residues, including C1782 and H1783, are located close to the active site (Extended Data Fig. 5a). Mutations of these residues did not affect the solubility of *cSPD*, but reduced the protease activity (Extended Data Fig. 5d). Moreover, residues from the tip of HI, along with residues from APD, form a basic pocket that binds a citrate molecule (Fig. 2f). Mutations of these conserved residues, with the exception of R1794E, diminished separase activity (Fig. 2e and Extended Data Fig. 1). Therefore, HI is critical for both the structure integrity and activity of separase.

Phosphorylation of *Scc1* by *Plk1* enhances *Scc1* cleavage by separase<sup>10,11</sup>. This cleavage-enhancing phosphorylation is opposed by the shugoshin-PP2A complex bound to cohesin<sup>23,27</sup>. Incubation of *cScc1*, but not *cScc1* S210A, with human *Plk1* (*hsPlk1*) enhanced the cleavage of *cScc1* by *cSPD* (Extended Data Fig. 6a). Addition of the *hsPlk1* inhibitor BI2536 blocked this enhancement. The phospho-mimicking S210E mutation stimulated *cScc1* cleavage by separase (Extended Data Fig. 6b). Thus, *Plk1*-dependent phosphorylation of *cScc1* at S210 enhances *Scc1* cleavage by separase.

We next determined the crystal structures of *cSPD* bound to unphosphorylated (AMK) or phospho-S210-containing (pAMK) inhibitors (Extended Data Table 1). The overall structure of *cSPD*-AMK and *cSPD*-pAMK complexes is virtually identical to that of free *cSPD*, indicating that substrate binding does not induce notable conformational changes. Only the C-terminal<sup>212</sup>EVGR<sup>215</sup> segment of the unphosphorylated AMK inhibitor was visible (Extended Data Fig. 6c), whereas all residues of the pAMK inhibitor had clearly defined electron density (Fig. 3a). In both structures, the active-site cysteine C2110 is covalently linked to *cScc1* R215 at the P1 position. Consistent with its role in stabilizing the oxyanion during catalysis, *cSPD* H2083 of the catalytic dyad is located close to carbonyl group of *cScc1* R215. R215 forms a salt bridge with *cSPD* D2151 at the base of a deep, acidic S1 pocket (Fig. 3b,c). *cScc1* E212 at P4 inserts into the aforementioned citrate-binding pocket, forming favorable electrostatic and hydrogen bonding interactions (Fig. 3b and Extended Data Fig. 6d). *cScc1* V213 and G214 form minimal contacts with *cSPD*. Mutations of residues lining the S1 and S4 pockets in *cSPD* greatly diminished separase activity (Fig. 3d).

The S1 pocket mutant D2151A of *cSPD* cleaved *cScc1* at a different site (Fig. 3d). The *cScc1* E180K mutation abolished this aberrant cleavage (Extended Data Fig. 6e), indicating that the mutant separase cleaved the<sup>180</sup>ELGM<sup>183</sup> site. Thus, D2151 not only selects for basic residues but also discriminates against hydrophobic residues at P1. *cSPD* charge reversal mutants D2151R and R2152E did not efficiently cleave the complementary charge reversal mutants of *cScc1* (Extended Data Fig. 6f), indicating that other residues in the S1 and S4 pockets contribute to substrate recognition. Because most residues lining the S1 and S4 pockets are conserved among separases in all species (Extended Data Figs. 1 and 7), our analyses establish the basis for the EXXR substrate specificity of separase.

Phosphorylation of the substrate does not alter the binding mode of EVGR at P1–P4, but reveals or establishes additional contacts at P5 and P6. I211 at the P5 position packs against W1797 of HI (Fig. 3e). *ctScc1* I211A was less efficiently cleaved by *ctSPD* with or without Plk1 (Extended Data Fig. 8a). Thus, as reported previously<sup>28</sup>, the hydrophobic residue at P5 contributes to substrate specificity. Phospho-S210 at P6 makes favorable electrostatic interactions with R1794 of HI and R2148 of APD in *ctSPD* (Fig. 3e and Extended Data Fig. 8b). Single mutation of R1794 or R2148 reduced the stimulation of Scc1 cleavage by Plk1, whereas the double mutation abolished the effect (Fig. 3f and Extended Data Fig. 8c,d). Unlike R2148A, R1794E does not affect the cleavage of unphosphorylated Scc1. Therefore, R1794 specifically serves as a receptor for pS210. R2148 contributes to the recognition of both pS210 and E212. The serine at P6 is conserved in fungal Scc1 and other separate substrates (Fig. 1b). The N-terminal separate cleavage site in vertebrate Scc1 contains a phospho-mimicking, acidic residue at that position. Our structures thus explain the phosphorylation dependency of cohesin cleavage, and further suggest that this phospho-regulation might apply to other separate substrates.

Finally, we probed the mechanism by which securin inhibits separate. Securin blocks substrate access to the active site of separate<sup>3,6</sup>. Expectedly, the *ctSecurin-ctSeparase* complex was less active in *ctScc1* cleavage, as compared to *ctSPD* (Extended Data Fig. 9a,b). A conserved EVE motif in securin matches the separate cleavage consensus at positions P2–P6, but lacks the arginine at P1 and often has a proline at P0 instead of a hydrophilic residue (Fig. 4a). A securin mutant with three residues in this motif mutated was cleaved by separate in fission yeast cells<sup>13</sup>. We thus mutated P164 and P165 in *ctSecurin* to R and D, the matching *ctScc1* residues at P1 and P0. The resulting *ctSecurin<sup>RD</sup>* mutant was efficiently cleaved by *ctSPD*, and this cleavage was inhibited by the AMK inhibitor (Fig. 4b). Mutating the phospho-serine-binding residues in *ctSPD* or E159 in *ctSecurin<sup>RD</sup>* reduced cleavage (Fig. 4c and Extended Data Fig. 9c), indicating that this artificial substrate bound at the canonical substrate-binding sites of separate. *ctSecurin* bound tightly to the N-terminal ARM domain of *ctSeparase* (Extended Data Fig. 9d). A synthetic EVE-containing securin peptide did not inhibit *ctSPD* (Extended Data Fig. 9e). We propose that securin acts as a pseudo-substrate to competitively block substrate binding to separate (Fig. 4d). Securin binding to the ARM domain of separate provides the necessary avidity for securin to outcompete authentic substrates for access to the active site. Securin is not cleaved because of incompatible residues at the site of cleavage.

As a crucial protease that triggers chromosome segregation, separate is a potential oncoprotein<sup>29</sup>. Because of the conserved principles of substrate recognition (Extended Data Fig. 7), our structure of an active fungal separate can guide the rational design of chemical inhibitors of human separate, which may have therapeutic potential.

## METHODS

### Expression and purification of *Chaetomium thermophilum* separate protease domain (*ctSPD*)

The *ct* separate cDNA (GenBank ID: 18261092) was synthesized at GenScript USA Inc. For the expression of the *ct* separate protease domain (*ctSPD*), the cDNA fragment of

*ctSPD*<sup>1632–2223</sup> was subcloned into a modified pET bacterial expression vector. The pET-*ctSPD* vector encoded *ctSPD*<sup>1632–2223</sup> with an N-terminal His<sub>6</sub> tag of the following sequence: MGSSHHHHHSQLEVLFGPLGSGRP. The pET-*ctSPD* vector was transformed into the *E. coli* strain BL21(DE3). Protein expression was induced with isopropylthiogalactoside (IPTG) at 18°C for overnight. The bacteria were harvested and resuspended in the lysis buffer (50 mM Tris-HCl, pH 8.0, 200 mM NaCl, 5% glycerol, 1 mM DTT, and 0.05% Triton X-100). After sonication and centrifugation, the supernatant was applied to Ni<sup>2+</sup>-NTA resin (Qiagen). After extensive washing, His<sub>6</sub>-*ctSPD* was eluted from the Ni<sup>2+</sup>-NTA column. His<sub>6</sub>-*ctSPD* was further purified with a mono Q 5/50 GL anion-exchange column (GE Healthcare) and a Superdex 200 10/300 GL column. The point mutants of *ctSPD* were generated with the QuikChange Lightning Site-Directed Mutagenesis kit (Agilent Technologies). The truncated variants and point mutants of *ctSPD* were expressed and purified similarly. Because *ctSPD*<sup>1632–2223</sup> underwent autocleavage at the <sup>1643</sup>ELAR<sup>1646</sup> site, we generated a noncleavable (NC) <sup>1643</sup>RLAE<sup>1646</sup> mutant to prevent autocleavage and increase yield. All *ctSPDs* in this study, except that in Extended Data Fig. 2b, contained the NC mutation.

The selenomethionine (SeMet)-labeled *ctSPD*<sup>1663–2223</sup> was produced with the methionine biosynthesis inhibition method<sup>31</sup>. Briefly, bacteria transformed with pET-*ctSPD* cultured overnight were pelleted, washed, and resuspended with M9 minimal media. The bacteria were further incubated at 37°C until the OD<sub>600</sub> reaches about 1.0. Methionine biosynthesis was inhibited by the addition of the amino acids solution containing 50 mg/l of Leu/Ile/Val and 100 mg/l of Phe/Lys/Thr/SeMet. Protein expression was induced with 0.4 mM IPTG at 18°C for overnight. The SeMet-labeled protein was subsequently purified through the same procedure as described above.

### Expression and purification of *ctSeparase*–*Securin* complex and *ctSPD*<sup>1501–2223</sup>

The *ctSecurin* cDNA (GenBank ID: 18256826) was cloned from a cDNA library of *Chaetomium thermophilum*. The cDNAs of *ctSeparase* and *ctSecurin* were separately subcloned into a modified pFastBac HT vector (Invitrogen). The final constructs encoded an N-terminal His<sub>6</sub>-Strep-tagged *ctSeparase* and an N-terminal His<sub>6</sub>-tagged *ctSecurin*. Baculoviruses of *ctSeparase* and *ctSecurin* were constructed with the Bac-to-Bac system (Invitrogen) according to the manufacturer's protocols. Sf9 cells were co-infected with *ctSeparase* and *ctSecurin* baculoviruses and harvested at 48 h post-infection. Cells were resuspended in the lysis buffer containing 50 mM Tris-HCl, pH 8.0, 200 mM NaCl, 5% glycerol, 1 mM DTT, and 0.05% Triton X-100, followed by sonication and centrifugation. The supernatant was applied onto a Strep-Tactin Superflow column (Qiagen). After extensive washes with the lysis buffer, the *ctSeparase*–*Securin* complex was eluted with the elution buffer containing 5 mM d-Desthiobiotin (Sigma-Aldrich), 50 mM Tris-HCl, pH 8.0, 200 mM NaCl, 5% glycerol, and 1 mM DTT. The His<sub>6</sub>-*ctSPD*<sup>1501–2223</sup> protein was expressed in Sf9 cells with a similar strategy and purified through a Ni<sup>2+</sup>-NTA column.

### Separase activity assay

The *ctScc1* cDNA (GenBank ID: 18259702) was synthesized by GenScript USA Inc. and was cloned into a modified pCS2 vector with a SP6 promoter. For producing <sup>35</sup>S-labeled

*c*Sccl or its mutants, the pCS2-*c*Sccl plasmids were added to the TNT Quick Coupled Transcription Translation System (Promega) and incubated in the presence of <sup>35</sup>S-methionine at 30°C for 90 min. (The <sup>35</sup>S-*c*Sccl proteins migrated as a doublet on SDS-PAGE, possibly due to proteolysis or internal methionine initiation during the *in vitro* translation reaction.) Then, 2 μl of <sup>35</sup>S-*c*Sccl was added to 18 μl of *c*SPD (~1.5 μM) or *c*Separase–Securin protein solution containing 25 mM HEPES (pH 7.5), 75 mM KCl, 5 mM MgCl<sub>2</sub>, 1 mM DTT, 15 mM NaF, 1 mM EGTA, 10% glycerol, and 0.05% Triton X-100, and incubated at 30°C for 60 min. For assays in Fig. 1c and Extended Data Fig. 2b, a higher concentration of *c*SPD (3.0 μM) was used, resulting in more complete *c*Sccl cleavage. For AMK inhibition assay, *c*SPD was pre-incubated with the *c*Sccl-AMK inhibitor (synthesized by KareBay Biochem, Inc) at room temperature for 30 min and further incubated with <sup>35</sup>S-*c*Sccl at 30°C for 60 min. In the Plk1 stimulation assay, <sup>35</sup>S-*c*Sccl was pre-treated with recombinant GST-*hs*Plk1<sup>T210D</sup> in the kinase buffer for 30 min at 30°C, in the absence or presence of 10 μM BI2536, and further incubated with *c*SPD (0.5 μM) for 60 min. The reaction mixtures were separated on SDS-PAGE gels, which were stained, destained, dried, and analyzed with Fuji or GE phosphoimagers.

The *c*Securin WT and P164R/P165D (*c*Securin<sup>RD</sup>) cDNAs were subcloned into pCS2-Myc vector with a SP6 promoter. The <sup>35</sup>S-labeled *c*Securin<sup>WT</sup> and *c*Securin<sup>RD</sup> proteins was produced and assayed as described above. The *c*Securin<sub>153–177</sub> (DPLQVEEVEYAPPKPKEMPYESDVF) and *c*Securin<sub>153–177</sub> 3A (DPLQVEAAA YAPPKPKEMPYESDVF) peptides were chemically synthesized and tested for their ability to inhibit the cleavage of *c*Sccl by *c*SPD as described above.

### Crystallization and data collection

All crystallization experiments were carried out at 20°C. Initial screens were performed with a Phoenix crystallization robot (Art Robbins Instruments), using the commercially available screening kits from Hampton Research, Qiagen, and Molecular Dimensions. Conditions obtained from the initial screens were optimized using hanging-drop vapor diffusion method. Diffraction-quality crystals were obtained by repeated microseeding. All crystals were cryoprotected with a reservoir solution supplemented with 15% glycerol.

Both native and SeMet-labeled *c*SPD<sup>1663–2223</sup> crystals were grown by mixing equal volumes of the protein solution (11 mg/ml) with the precipitant solution containing 0.2 M ammonium citrate tribasic (pH 7.0), 20% PEG3350, and 10 mM DTT. Diffraction data were collected at beamline BL8.2.1 at the Advanced Light Source (Lawrence Berkeley National Laboratory) at the wavelength of 0.9786 Å at 100 K and processed with HKL3000<sup>32</sup>.

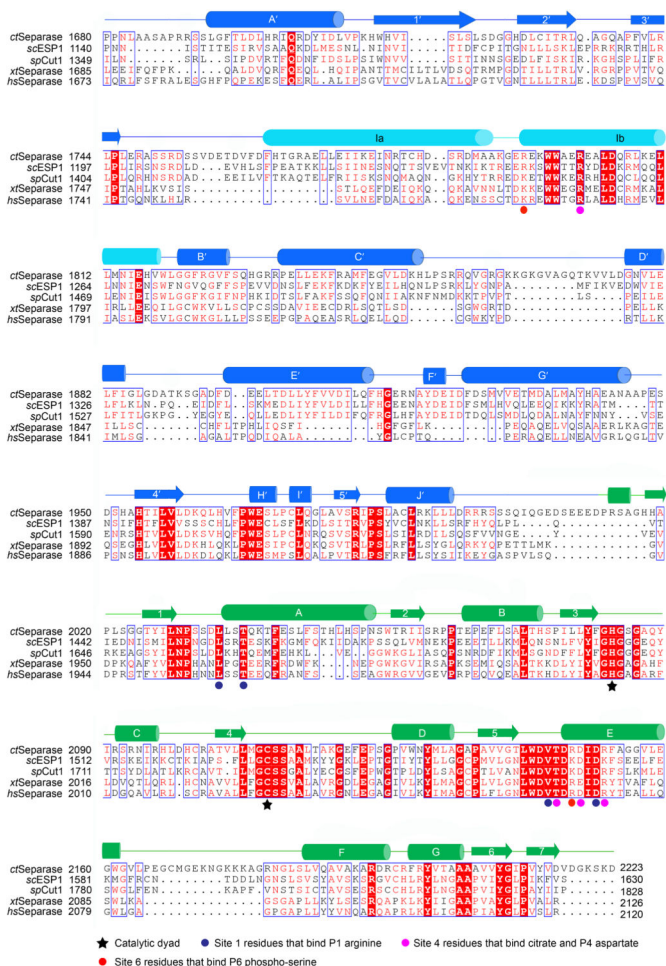
For crystallization of *c*SPD<sup>1632–2223</sup>-AMK and *c*SPD<sup>1693–2223</sup>-pAMK complexes, the purified *c*SPD proteins were mixed with the *c*Sccl-AMK or phospho-*c*Sccl-AMK peptide inhibitors (KareBay Biochem) at a molar ratio of 1:2.5, and incubated overnight at room temperature to form covalent complexes as monitored by SDS-PAGE. The complexes were further purified with a Superdex 200 10/300 GL size exclusion column in the buffer containing 20 mM Tris-HCl (pH 8.0), 200 mM NaCl, and 5 mM DTT. Crystals of *c*SPD<sup>1632–2223</sup>-AMK were grown by mixing equal volumes of the protein solution (13 mg/ml) with the precipitant solution containing 0.1 M ammonium citrate tribasic (pH 7.0)

and 12% PEG3350. For the crystallization of *c*tSPD<sup>1693–2223</sup>-pAMK complex, the 11 mg/ml protein solution was mixed with an equal volume of the precipitant solution containing 0.2 M KCl, 50 mM HEPES (pH 7.5), 32% pentaerythritol propoxylate (5/4 PO/OH), and 10 mM DTT. Diffraction data for *c*tSPD<sup>1632–2223</sup>-AMK and *c*tSPD<sup>1693–2223</sup>-pAMK were collected at beamline 19-ID (SBC-CAT) at the Advanced Photon Source (Argonne National Laboratory) at 100 K at the wavelengths of 0.9793 Å and 0.9795 Å, respectively, and processed with HKL3000.

### Structure determination and refinement

The crystal of SeMet-labeled *c*tSPD<sup>1663–2223</sup> diffracted to a minimum Bragg's spacing of 2.20 Å and exhibited the symmetry of the space group P212121 with cell dimensions of a = 55.67 Å, b = 98.79 Å, c = 107.76 Å. Phases were obtained from the selenium single anomalous dispersion (SAD) method. With data truncated to 2.5 Å, 9 of 10 possible selenium sites were located and refined with PHENIX AutoSol<sup>33</sup>, resulting in an overall figure of merit of 0.323. The experimental electron density map was used to construct an initial model with automated building with PHENIX AutoBuild. As a result, 414 of total 587 residues were built in the initial model, with  $R_{\text{work}}$  and  $R_{\text{free}}$  of 27.74% and 32.79%, respectively. Iterative model building and refinement were carried out with JLigand<sup>34</sup>, COOT<sup>35</sup> and PHENIX, respectively. Phases of native *c*tSPD<sup>1663–2223</sup>, *c*tSPD<sup>1632–2223</sup>-AMK, and *c*tSPD<sup>1693–2223</sup>-pAMK were obtained by molecular replacement with Phaser using the SeMet crystal structure as the search model. Data collection and structure refinement statistics are summarized in Extended Data Table 1. Ramachandran statistics (Favored/allowed/outlier (%)) calculated by MolProbity<sup>36</sup> for *c*tSPD<sup>1663–2223</sup>, *c*tSPD<sup>1632–2223</sup>-AMK and *c*tSPD<sup>1693–2223</sup>-pAMK are 98.0/1.6/0.4, 98.1/1.9/0.0 and 98.1/1.7/0.2, respectively. All structural figures are generated with the program PyMOL (<http://www.pymol.org/>) using the same color and labeling schemes.

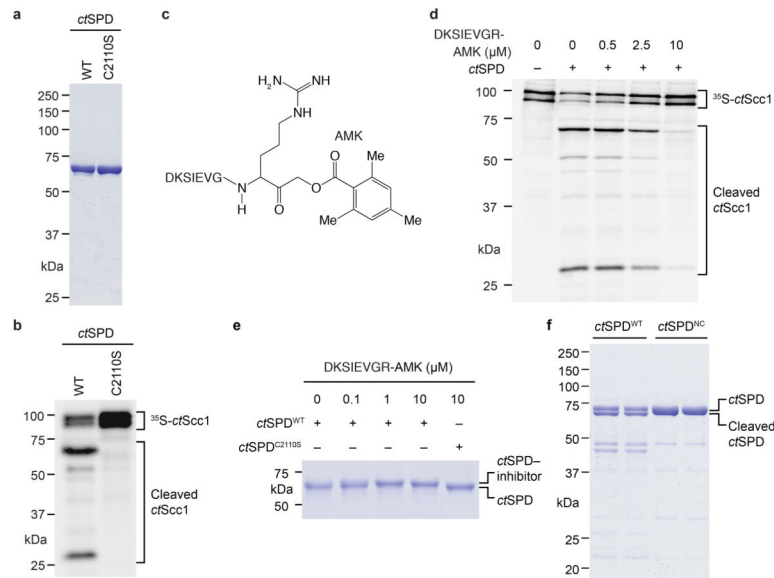
Extended Data



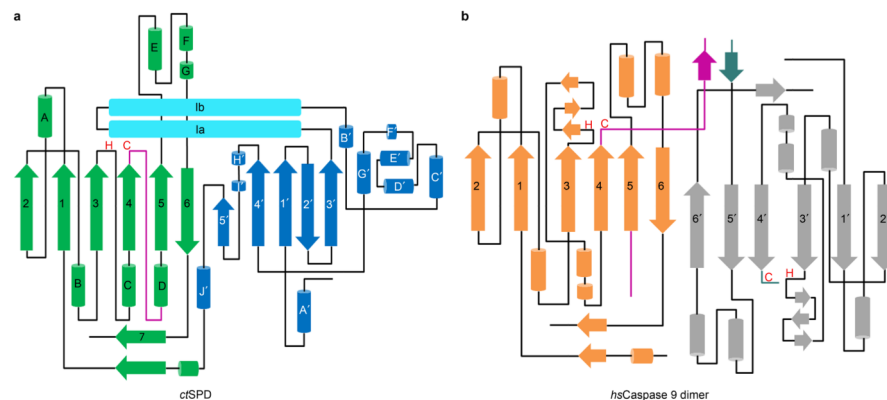
**Extended Data Figure 1. Sequence alignment of the separase protease domains (SPD) from multiple species**

The alignment is generated using the online ESPrict 2.0 server. Secondary structural elements of *ct*SPD are indicated above the sequences, with the same labeling and color schemes as in Fig. 1d (PPD, blue; APD, green; the helical insert in PPD, cyan). *ct*, *Chaetomium thermophilum*; *sc*, *Saccharomyces cerevisiae*; *sp*, *Schizosaccharomyces pombe*; *xt*, *Xenopus tropicalis*; *hs*, *Homo sapiens*.

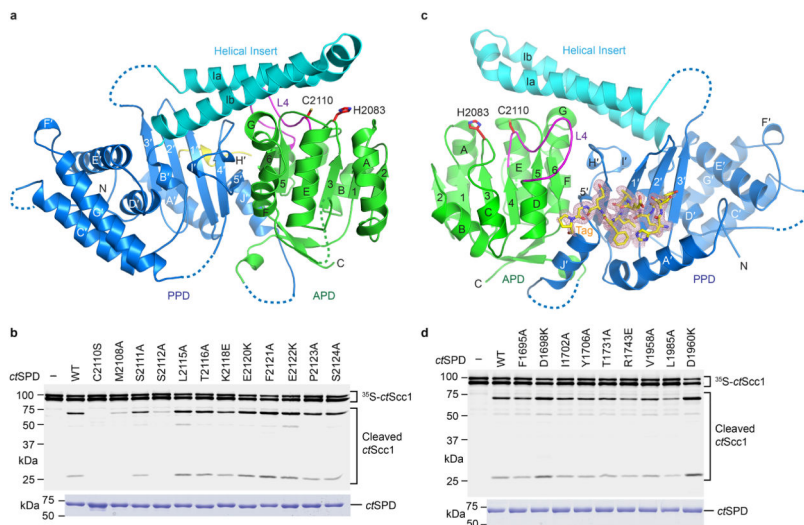




**Extended Data Figure 2. Purification, activity, inhibition, and autocleavage of active *ctSPD***  
**a.** Coomassie-stained gel of purified recombinant *ctSPD* wild type (WT) and C2110S. **b.** Autoradiograph of the *ctSPD* cleavage assay with  $^{35}\text{S}$ -*ctScc1* as substrate. **c.** Chemical structure of the acyloxymethyl ketone (AMK) inhibitor derived from the *ctScc1* cleavage site. **d.** Autoradiograph of the *ctSPD* cleavage assay with  $^{35}\text{S}$ -*ctScc1* as substrate, in the absence or presence of increasing doses of the AMK inhibitor depicted in **c.** **e.** Coomassie-stained SDS-PAGE gel of purified recombinant *ctSPD* WT or C2110S treated with the indicated doses of the *ctScc1*-AMK peptide inhibitor. The positions of unmodified *ctSPD* and *ctSPD*-inhibitor conjugates are indicated. **f.** Coomassie-stained gel of recombinant *ctSPD*<sup>1632–2223</sup> WT or noncleavable (NC) mutant. The *ctSPD*<sup>NC</sup> mutant contains the E1643R and R1646E mutations. The positions of intact and autocleaved *ctSPD* proteins are indicated.

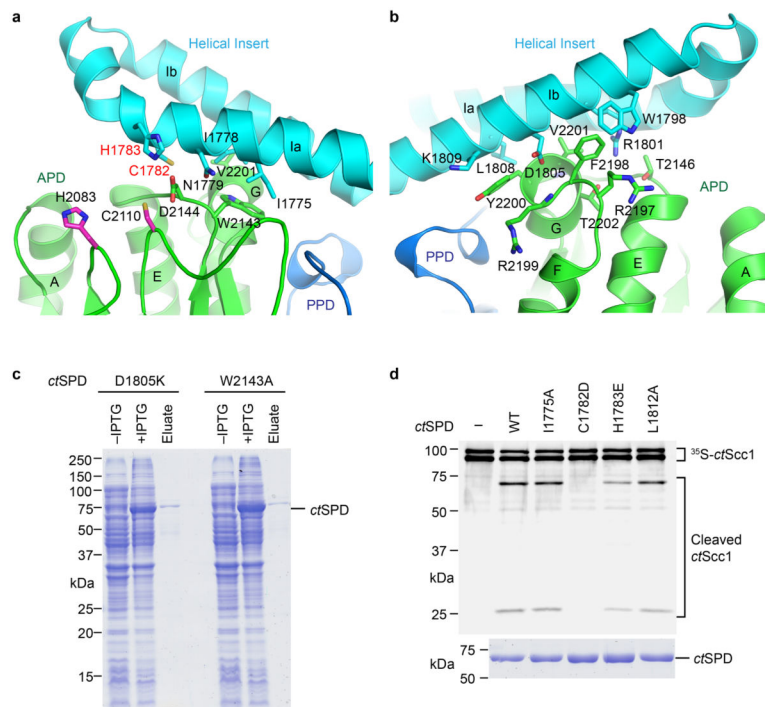


**Extended Data Figure 3. Comparison between the folding topologies of *ctSPD* and the caspase 9 dimer (PDB: 1JXQ)**  
The labeling and color schemes are the same as in Fig. 1d,e. H, the catalytic histidine; C, the catalytic cysteine.

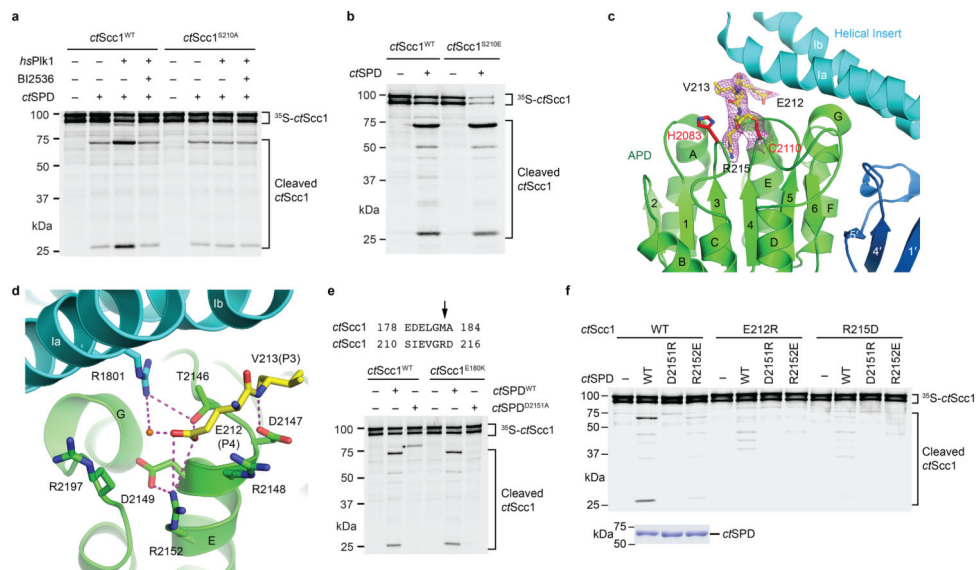


**Extended Data Figure 4. Contributions of the L4 loop and a surface pocket to the protease activity of *ctSPD***

**a**, Cartoon diagram of the crystal structure of *ctSPD*, with the pseudo protease domain (PPD) colored blue, the active domain (APD) colored green, the helical insert in PPD colored cyan, and an N-terminal tag peptide colored yellow. The N- and C-termini are indicated. All secondary structure elements are labeled. Loops with no visible electron densities are indicated by dashed lines. Loop 4 (L4) is colored magenta. H2083 and C2110 of the catalytic dyad are shown as sticks. The orientation of *ctSPD* in this figure is related to that Fig. 1d by a 180° rotation along the vertical axis. **c**, Representative autoradiograph of the <sup>35</sup>S-*ctScc1* cleavage assay by WT *ctSPD* or the indicated mutants. The bottom panel shows a Coomassie-stained gel of *ctSPD* proteins used in the assay. Quantification of the relative protease activities of *ctSPD* WT and mutants is shown in Fig. 2b. The protease activity is defined as the ratio between intensities of the two major *ctScc1* cleavage products and that of the uncleaved *ctScc1*. **c**, Cartoon diagram of the crystal structure of *ctSPD*, in the same orientation as in Fig. 1d. The tag peptide (HSQLEVLFGQP) is shown as sticks, overlaid with its 2Fo-Fc electron density map contoured at 1.0 σ. **d**, Representative autoradiograph of the <sup>35</sup>S-*ctScc1* cleavage assay by WT *ctSPD* or the indicated mutants. The bottom panel shows a Coomassie-stained gel of *ctSPD* proteins used in the assay. Quantification of the relative protease activities of *ctSPD* WT and mutants is shown in Fig. 2d.

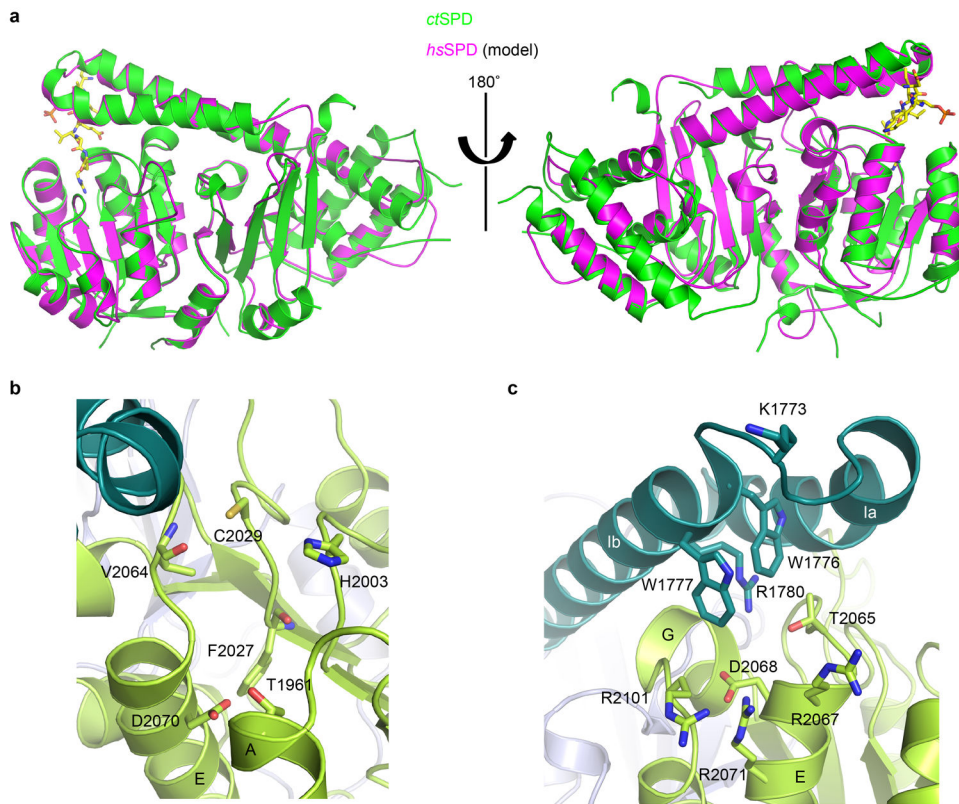


**Extended Data Figure 5. Interactions between the helical insert and the active protease domain** **a,b**, Zoomed in views of cartoon diagrams of *ctSPD* in two orientations that are related by a 180° rotation along the vertical axis. Residues at the interface between the helical insert of the pseudo protease domain (PPD) and the active protease domain (APD) are shown in sticks and labeled. **c**, Coomassie-stained gel of lysates of bacteria expressing the indicated *ctSPD* mutants and treated without (–) or with (+) isopropyl β-D-1-thiogalactopyranoside (IPTG) and eluates from Ni<sup>2+</sup>-NTA beads that had been incubated with the IPTG lysates. **d**, Autoradiograph of the <sup>35</sup>S-*ctScc1* cleavage assay by WT *ctSPD* or the indicated mutants. The bottom panel shows a Coomassie-stained gel of *ctSPD* proteins used in the assay.

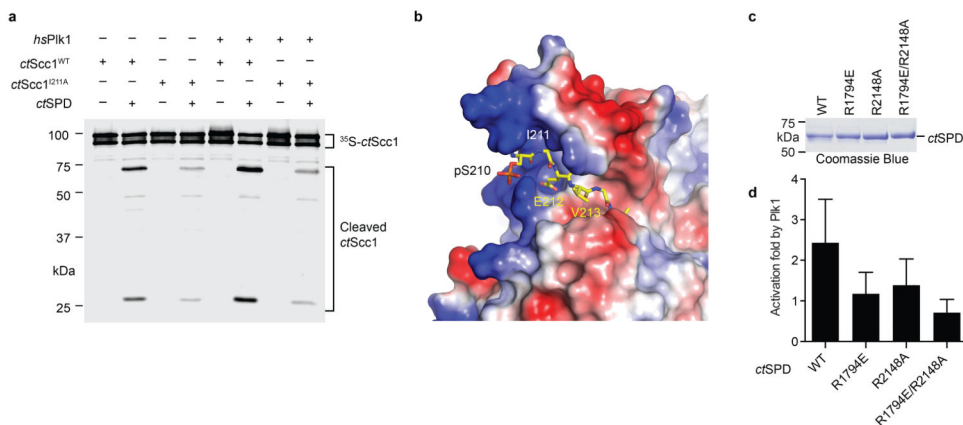


### Extended Data Figure 6. Phospho-regulation and specificity determinants of separase-mediated cohesin cleavage

**a**, Autoradiograph of the *cfSPD* cleavage reactions of <sup>35</sup>S-*cfScs1* WT or S210A, treated with or without human (*hs*) Plk1 or its inhibitor BI2536. **b**, Autoradiograph of the *cfSPD* cleavage reactions, with <sup>35</sup>S-*cfScs1* WT or the phospho-mimicking S210E as substrates. **c**, Zoomed-in view of the cartoon diagram of *cfSPD* bound covalently to the *cfScs1*-AMK inhibitor. The catalytic dyad C2110 and H2083 are shown as red sticks. The covalently bound inhibitor is shown as yellow sticks, overlaid with its 2Fo-Fc electron density map contoured at 1.0  $\sigma$ . **d**, Zoomed-in view of the S4 pocket of *cfSPD* that recognizes the P4 glutamate. Dashed lines indicate hydrogen bonds or favorable electrostatic interactions. The orange sphere indicates a water molecule. **e**, Mapping of the aberrant *cfScs1* cleavage site by *cfSPD* D2151A. Top panel, sequence alignment of the aberrant site of D2151A and the major site of WT. Bottom panel, autoradiograph of the cleavage reactions of *cfSPD*<sup>WT</sup> or *cfSPD*<sup>D2151A</sup> with the indicated <sup>35</sup>S-*cfScs1* proteins as substrates. Asterisk marks the aberrant cleavage product by *cfSPD*<sup>D2151A</sup>. **f**, Charge reversal mutants of *cfSPD* fail to cleave complementary charge reversal mutants of *cfScs1*. Autoradiograph of the cleavage assay of WT *cfSPD* or the indicated mutants, with <sup>35</sup>S-*cfScs1* WT or mutants as substrates. The bottom panel shows a Coomassie-stained gel of *cfSPD* proteins used in the assay.

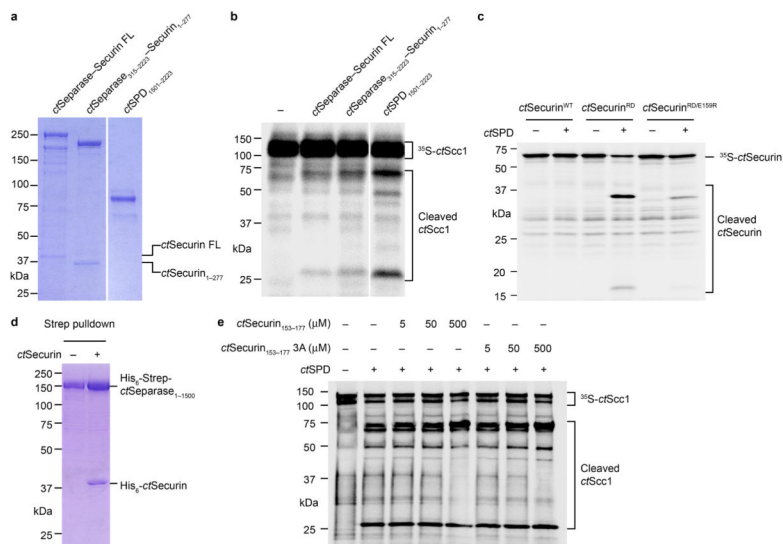


**Extended Data Figure 7. Conservation of substrate-binding residues in human separase**  
**a**, Two different views of the cartoon diagram of the structure of *ct*SPD–pAMK (green) and a homology model of human (*hs*) SPD (magenta). The phospho-AMK peptide is shown in sticks. The homology model of *hs*SPD was generated with SWISS-MODEL. The coordinates of the model are available upon request. **b,c**, Zoomed-in views of the S1 and S4 pockets of the *hs*SPD model.



**Extended Data Figure 8. Structural basis of phosphorylation-stimulated Scc1 cleavage**  
**a**, Autoradiograph of the *ct*SPD cleavage reactions of <sup>35</sup>S-*ct*Scc1 WT or I211A, treated with or without *hs*Plk1. **b**, Zoomed-in view of the surface drawing of *ct*SPD–pAMK. The surface

is colored according to the electrostatic potential, with red, blue, and white representing negative, positive, and neutral charges, respectively. The covalently bound peptide is shown as sticks. **c**, Coomassie-stained gel of the indicated *ctSPD* proteins used in the assays described in Figs. 3f and 4c. **d**, Quantification of the fold of Plk1 stimulation in *ctScc1* cleavage by *ctSPD* WT and the indicated mutants as described in Fig. 3f. Error bars, s.d. ( $n = 3$  independent experiments).



#### Extended Data Figure 9. Interactions between *ctSecurin* and *ctSeparase*

**a**, Coomassie-stained gel of recombinant *ctSeparase*–*ctSecurin* complexes and the *ctSeparase* Protease Domain (*ctSPD*) expressed in insect cells. FL, full length. **b**, Autoradiograph of the *ctScc1* cleavage reactions by the *ctSeparase*–*ctSecurin* complexes and *ctSPD*. **c**, Autoradiograph of the cleavage reactions of  $^{35}\text{S}$ -*ctSecurin* WT or mutants with or without *ctSPD*. **d**, Coomassie-stained gel of recombinant Strep-tagged *ctSeparase*<sub>1–1500</sub> or the *ctSeparase*<sub>1–1500</sub>–*ctSecurin* complex bound to Strep-Tactin beads. **e**, Autoradiograph of the *ctScc1* cleavage reactions by *ctSPD*, in the absence or presence of varying concentrations of the *ctSecurin*<sub>153–177</sub> or *ctSecurin*<sub>153–177</sub> 3A peptides. The EVE motif is mutated to AAA in the *ctSecurin*<sub>153–177</sub> 3A peptide.

#### Extended Data Table 1

Data collection and refinement statistics

	<i>ctSPD</i> <sup>1663–2223</sup>	<i>ctSPD</i> <sup>1632–2223</sup> –AMK	<i>ctSPD</i> <sup>1693–2223</sup> –pAMK
<b>Data collection</b>			
Space group	P2 <sub>1</sub> 2 <sub>1</sub> 2 <sub>1</sub>	P6 <sub>3</sub> 22	P2 <sub>1</sub> 2 <sub>1</sub> 2 <sub>1</sub>
Cell dimensions			
<i>a</i> , <i>b</i> , <i>c</i> (Å)	55.56, 98.89, 107.75	149.15, 149.15, 115.63	56.35, 85.01, 119.27
<i>α</i> , <i>β</i> , <i>γ</i> (°)	90, 90, 90	90, 90, 120	90, 90, 90
Resolution (Å)	50.00–1.90 (1.93–1.90)*	50.00–3.10 (3.15–3.10)	50.00–1.85 (1.88–1.85)
<i>R</i> <sub>merge</sub> (%)	7.4 (97.0)	15.5 (100)	13.5 (100)

	<i>ctSPD</i> <sup>1663–2223</sup>	<i>ctSPD</i> <sup>1632–2223</sup> -AMK	<i>ctSPD</i> <sup>1693–2223</sup> -pAMK
<i>I</i> / $\sigma$ <i>I</i>	27.7 (2.5)	14.6 (1.3)	19.8 (1.9)
Completeness (%)	100 (100)	99.9 (98.7)	100 (100)
Redundancy	7.2 (7.3)	9.6 (8.7)	7.5 (5.8)
<b>Refinement</b>			
Resolution (Å)	49.38-1.90	48.82-3.10	42.51-1.85
No. reflections	46925	14228	50139
<i>R</i> <sub>work</sub> / <i>R</i> <sub>free</sub>	17.3/20.0	19.4/25.8	18.0/20.7
No. atoms			
Protein	3937	3745	3730
Ligand/ion	13	36	134
Water	394	52	454
<i>B</i> -factors			
Protein	27.4	78.4	26.6
Ligand/ion	32.6	86.0	29.8
Water	37.1	66.3	38.4
R.m.s deviations			
Bond lengths (Å)	0.012	0.010	0.013
Bond angles (°)	1.24	1.13	1.05

Data were collected from one crystal for each structure.

\*Highest-resolution shell is shown in parenthesis.

## Supplementary Material

Refer to Web version on PubMed Central for supplementary material.

## Acknowledgments

We thank D. Rosenbaum for the *Chaetomium thermophilum* cDNA, H. Ball for peptide synthesis, and D. Tomchick and Z. Chen for assistance with data collection. Diffraction data of the selenomethionine separase were collected at the Advanced Light Source at Lawrence Berkeley National Laboratory with the help of its staff. The Advanced Light Source is supported by the Director, Office of Science, Office of Basic Energy Sciences, of the U.S. Department of Energy under Contract No. DE-AC02-05CH11231. Results shown in this report are derived from work performed at Argonne National Laboratory, Structural Biology Center at the Advanced Photon Source. Argonne is operated by UChicago Argonne, LLC, for the U.S. Department of Energy, Office of Biological and Environmental Research under contract DE-AC02-06CH11357. This work is supported by the Cancer Prevention and Research Institute of Texas (RP110465-P3 to H.Y.), the National Institutes of Health (GM107415 to X.L.), and the Welch Foundation (I-1441 to H.Y.). H.Y. is an investigator with the Howard Hughes Medical Institute.

## References

1. Uhlmann F, Wernic D, Poupart MA, Koonin EV, Nasmyth K. Cleavage of cohesin by the CD clan protease separin triggers anaphase in yeast. *Cell*. 2000; 103:375–386. [PubMed: 11081625]
2. Hauf S, Waizenegger IC, Peters JM. Cohesin cleavage by separase required for anaphase and cytokinesis in human cells. *Science*. 2001; 293:1320–1323. [PubMed: 11509732]
3. Hornig NC, Knowles PP, McDonald NQ, Uhlmann F. The dual mechanism of separase regulation by securin. *Curr Biol*. 2002; 12:973–982. [PubMed: 12123570]
4. Ciosk R, et al. An ESP1/PDS1 complex regulates loss of sister chromatid cohesion at the metaphase to anaphase transition in yeast. *Cell*. 1998; 93:1067–1076. [PubMed: 9635435]

5. Zou H, McGarry TJ, Bernal T, Kirschner MW. Identification of a vertebrate sister-chromatid separation inhibitor involved in transformation and tumorigenesis. *Science*. 1999; 285:418–422. [PubMed: 10411507]
6. Waizenegger I, Gimenez-Abian JF, Wernic D, Peters JM. Regulation of human separase by securin binding and autocleavage. *Curr Biol*. 2002; 12:1368–1378. [PubMed: 12194817]
7. Stemmann O, Zou H, Gerber SA, Gygi SP, Kirschner MW. Dual inhibition of sister chromatid separation at metaphase. *Cell*. 2001; 107:715–726. [PubMed: 11747808]
8. Gorr IH, Boos D, Stemmann O. Mutual inhibition of separase and Cdk1 by two-step complex formation. *Mol Cell*. 2005; 19:135–141. [PubMed: 15989971]
9. Hellmuth S, et al. Human chromosome segregation involves multi-layered regulation of separase by the peptidyl-prolyl-isomerase Pin1. *Mol Cell*. 2015; 58:495–506. [PubMed: 25921067]
10. Alexandru G, Uhlmann F, Mechtler K, Poupard MA, Nasmyth K. Phosphorylation of the cohesin subunit Scc1 by Polo/Cdc5 kinase regulates sister chromatid separation in yeast. *Cell*. 2001; 105:459–472. [PubMed: 11371343]
11. Hauf S, et al. Dissociation of cohesin from chromosome arms and loss of arm cohesion during early mitosis depends on phosphorylation of SA2. *PLoS Biol*. 2005; 3:e69. [PubMed: 15737063]
12. Katis VL, et al. Rec8 phosphorylation by casein kinase 1 and Cdc7-Dbf4 kinase regulates cohesin cleavage by separase during meiosis. *Dev Cell*. 2010; 18:397–409. [PubMed: 20230747]
13. Nagao K, Yanagida M. Securin can have a separase cleavage site by substitution mutations in the domain required for stabilization and inhibition of separase. *Genes Cells*. 2006; 11:247–260. [PubMed: 16483313]
14. Viadiu H, Stemmann O, Kirschner MW, Walz T. Domain structure of separase and its binding to securin as determined by EM. *Nat Struct Mol Biol*. 2005; 12:552–553. [PubMed: 15880121]
15. Gligoris TG, et al. Closing the cohesin ring: structure and function of its Smc3-kleisin interface. *Science*. 2014; 346:963–967. [PubMed: 25414305]
16. Huis in 't Veld PJ, et al. Characterization of a DNA exit gate in the human cohesin ring. *Science*. 2014; 346:968–972. [PubMed: 25414306]
17. Sullivan M, Lehane C, Uhlmann F. Orchestrating anaphase and mitotic exit: separase cleavage and localization of Slk19. *Nat Cell Biol*. 2001; 3:771–777. [PubMed: 11533655]
18. Matsuo K, et al. Kendrin is a novel substrate for separase involved in the licensing of centriole duplication. *Curr Biol*. 2012; 22:915–921. [PubMed: 22542101]
19. Renshaw MW, Stenicek HR, Scott FL, Liddington RC, Salvesen GS. Dimer formation drives the activation of the cell death protease caspase 9. *Proc Natl Acad Sci U S A*. 2001; 98:14250–14255. [PubMed: 11734640]
20. Chai J, et al. Structural basis of caspase-7 inhibition by XIAP. *Cell*. 2001; 104:769–780. [PubMed: 11257230]
21. Srinivasula SM, Ahmad M, Fernandes-Alnemri T, Alnemri ES. Autoactivation of procaspase-9 by Apaf-1-mediated oligomerization. *Mol Cell*. 1998; 1:949–957. [PubMed: 9651578]
22. Shi Y. Caspase activation: revisiting the induced proximity model. *Cell*. 2004; 117:855–858. [PubMed: 15210107]
23. Kitajima TS, et al. Shugoshin collaborates with protein phosphatase 2A to protect cohesin. *Nature*. 2006; 441:46–52. [PubMed: 16541025]
24. Riedel CG, et al. Protein phosphatase 2A protects centromeric sister chromatid cohesion during meiosis I. *Nature*. 2006; 441:53–61. [PubMed: 16541024]
25. Tang Z, et al. PP2A is required for centromeric localization of Sgo1 and proper chromosome segregation. *Dev Cell*. 2006; 10:575–585. [PubMed: 16580887]
26. Ishiguro T, Tanaka K, Sakuno T, Watanabe Y. Shugoshin-PP2A counteracts casein-kinase-1-dependent cleavage of Rec8 by separase. *Nat Cell Biol*. 2010; 12:500–506. [PubMed: 20383139]
27. Liu H, Rankin S, Yu H. Phosphorylation-enabled binding of SGO1-PP2A to cohesin protects sororin and centromeric cohesion during mitosis. *Nat Cell Biol*. 2013; 15:40–49. [PubMed: 23242214]
28. Sullivan M, Hornig NC, Porstmann T, Uhlmann F. Studies on substrate recognition by the budding yeast separase. *J Biol Chem*. 2004; 279:1191–1196. [PubMed: 14585836]



29. Zhang N, et al. Overexpression of Separase induces aneuploidy and mammary tumorigenesis. *Proc Natl Acad Sci U S A*. 2008; 105:13033–13038. [PubMed: 18728194]
30. Sun Y, et al. Separase is recruited to mitotic chromosomes to dissolve sister chromatid cohesion in a DNA-dependent manner. *Cell*. 2009; 137:123–132. [PubMed: 19345191]
31. Van Duyne GD, Standaert RF, Karplus PA, Schreiber SL, Clardy J. Atomic structures of the human immunophilin FKBP-12 complexes with FK506 and rapamycin. *J Mol Biol*. 1993; 229:105–124. [PubMed: 7678431]
32. Minor W, Cymborowski M, Otwinowski Z, Chruszcz M. HKL-3000: the integration of data reduction and structure solution—from diffraction images to an initial model in minutes. *Acta Crystallogr D Biol Crystallogr*. 2006; 62:859–866. [PubMed: 16855301]
33. Adams PD, et al. PHENIX: a comprehensive Python-based system for macromolecular structure solution. *Acta Crystallogr D Biol Crystallogr*. 2010; 66:213–221. [PubMed: 20124702]
34. Lebedev AA, et al. JLigand: a graphical tool for the CCP4 template-restraint library. *Acta Crystallogr D Biol Crystallogr*. 2012; 68:431–440. [PubMed: 22505263]
35. Emsley P, Cowtan K. Coot: model-building tools for molecular graphics. *Acta Crystallogr D Biol Crystallogr*. 2004; 60:2126–2132. [PubMed: 15572765]
36. Chen VB, et al. MolProbity: all-atom structure validation for macromolecular crystallography. *Acta Crystallogr D Biol Crystallogr*. 2010; 66:12–21. [PubMed: 20057044]

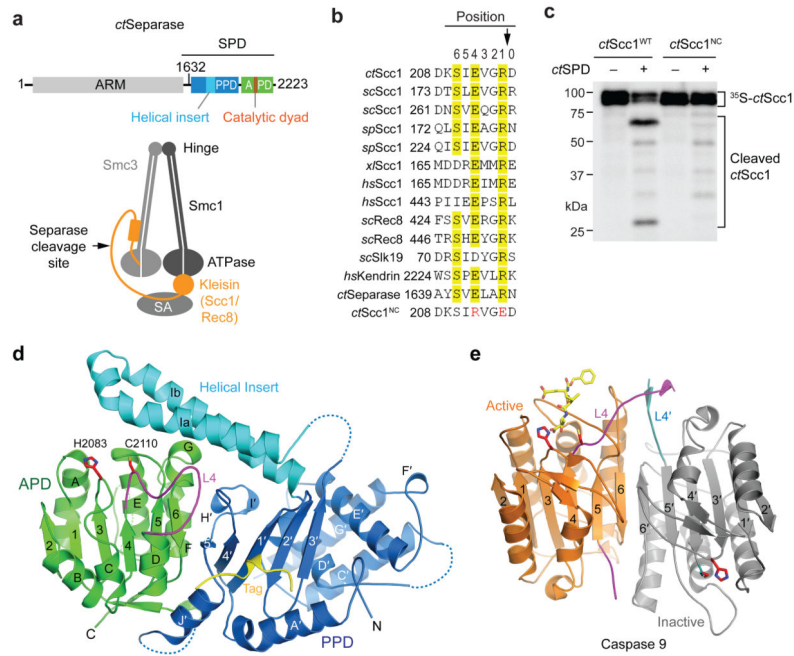


**Figure 1. Structure of *Chaetomium thermophilum* separase protease domain (*ctSPD*)**

**a**, Domains and motifs of separase from the thermophilic fungus *Chaetomium thermophilum* (*ct*) (top panel) and schematic drawing of cohesin (bottom panel). **b**, Sequence alignment of the cleavage sites of separase substrates. **c**, Autoradiograph of the *ctSPD* cleavage assay with <sup>35</sup>S-*ctScc1* wild type (WT) or non-cleavable mutant (NC) as substrates. For gel source data, see Supplementary Fig. 1. **d**, Cartoon diagram of the crystal structure of *ctSPD*. L4 is colored magenta. Loops with no visible electron densities are indicated by dashed lines. **e**, Cartoon diagram of caspase 9 (PDB: 1JXQ), with the bound inhibitor shown as yellow sticks.

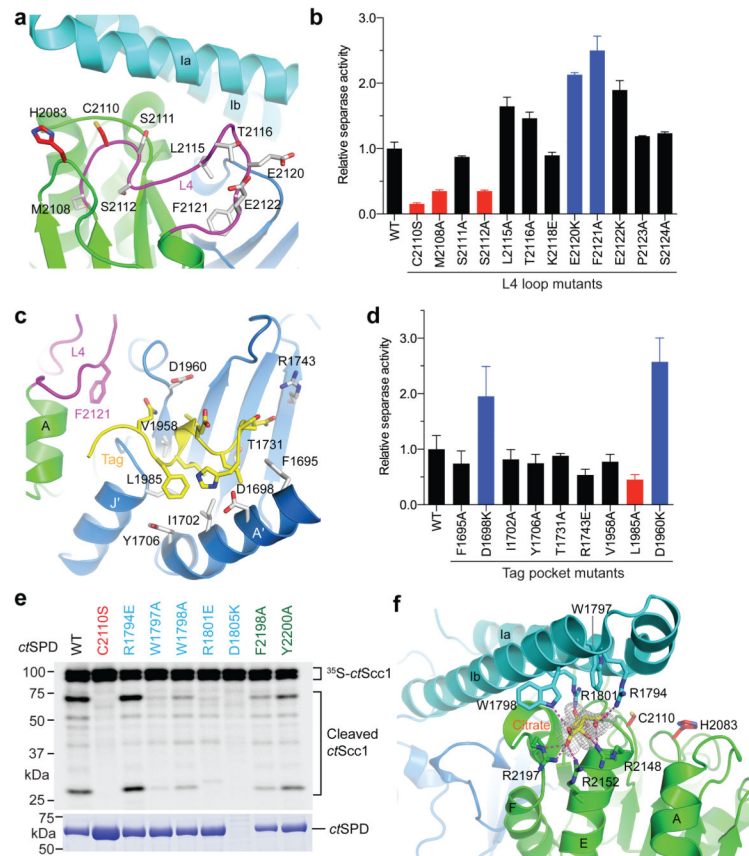


**Figure 2. Contributions of the L4 loop and helical insert to the activity of *cfSPD***  
**a**, Cartoon diagram of *cfSPD* with the catalytic dyad and L4 loop residues shown. **b,d**, Quantification of the protease activity of *cfSPD* WT and mutants (mean  $\pm$  s.d.,  $n = 3$  independent experiments). Mutants with activities greater or less than two-fold of WT are in blue and red, respectively. **c**, Interactions between the N-terminal tag and a surface pocket of *cfSPD*. **e**, Autoradiograph of the  $^{35}\text{S}$ -*cfScc1* cleavage assay by *cfSPD* WT or mutants. The bottom panel shows a Coomassie-stained gel of *cfSPD* proteins. **f**, A conserved basic pocket in *cfSPD*, with the 2Fo-Fc map of the bound citrate shown at  $2.0 \sigma$ .

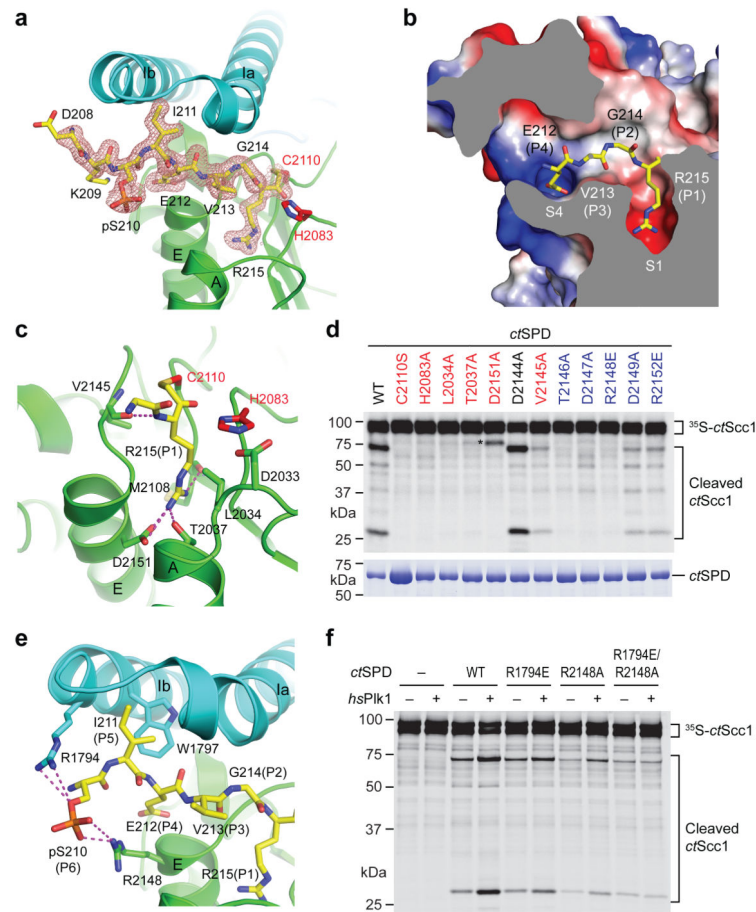


### Figure 3. Structural basis of Scc1 cleavage by separase

**a.** Cartoon diagram of *c*SPD bound to pAMK (shown as sticks overlaid with the 2Fo-Fc map at 1.0  $\sigma$ ). **b.** Cross-sectional view of the surface drawing of *c*SPD–*c*Scc1 colored with its electrostatic potential (blue, positive; red, negative; white, neutral). The bound Scc1 peptide is shown as sticks. **c.** The S1 pocket of *c*SPD that recognizes the P1 arginine. Dashed lines indicate hydrogen bonds or favorable electrostatic interactions. **d.** Autoradiograph of the cleavage reaction of *c*SPD WT and mutants with  $^{35}\text{S}$ -*c*Scc1 as substrate. Active-site/S1 mutants are labeled red; S4 mutants are labeled blue. Bottom panel, Coomassie-stained gel of the *c*SPD proteins. Asterisk marks an aberrant cleavage product of D2151A. **e.** The pS210-binding site. **f.** Autoradiograph of the cleavage reactions of *c*SPD WT and mutants with  $^{35}\text{S}$ -*c*Scc1 as substrate, with or without a prior incubation with *hs*Plk1.

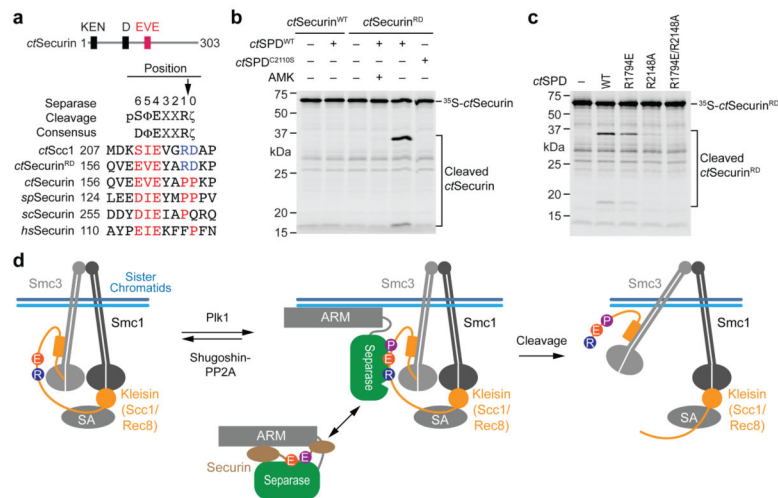


#### Figure 4. Securin as a pseudo-substrate of separase

**a**, Sequence alignment of the EVE motif of securin, with the separase cleavage consensus shown above. The KEN and destruction boxes (D) are indicated. Φ/ζ, hydrophobic/hydrophilic residues. **b**, Autoradiograph of the cleavage reactions of <sup>35</sup>S-*c*Securin WT or P164R/P165D (RD) by *c*SPD WT or C2110S with or without the AMK inhibitor. **c**, Autoradiograph of the cleavage reactions of <sup>35</sup>S-*c*Securin<sup>RD</sup> by the indicated *c*SPD proteins. **d**, Model depicting specificity determinants, phospho-regulation, and securin inhibition of separase-dependent cohesin cleavage. SA, stromal antigen. Cohesin cleavage by separase can be stimulated by DNA<sup>30</sup>. The ARM domain of separase might contact DNA.